hep-ph/9903439
DTP/99/28
March 1999

Small x QCD effects in DIS with a forward jet or a forward π^0.

J. Kwieciński[a,b], A.D. Martin[a] and J.J. Outhwaite[a].

[a] Department of Physics, University of Durham, Durham, DH1 3LE, UK.
[b] H. Niewodniczanski Institute of Nuclear Physics, ul. Radzikowskiego 152, 31-342 Krakow, Poland.

arXiv:hep-ph/9903439v2 28 Apr 1999

Abstract

We compare predictions based on small x (QCD) dynamics with recent data for deep inelastic events containing forward jets or forward π^0 mesons. We quantify the effect of imposing the (higher order) consistency condition on the BFKL equation and study uncertainties inherent in the QCD predictions. We also estimate the cross-section for the forward production of two jets.

1 Introduction

The positron-proton collider at HERA in the DESY facility has opened a window on a rich vein of fascinating physics. In recent years the range of the available kinematic space for deep inelastic processes has been extended ever further, and for a greater breadth of processes, allowing for increasingly stringent tests on the physics of Quantum Chromodynamics (QCD), the theory of strong interactions, at perturbative energies.

Pertubative QCD allows us to predict the evolution in kinematic space (but not the initial form) of the parton distribution functions. These in turn drive the equations that describe physical observables. In distinct regions of (x, Q^2) space we have two different modes of parton evolution. At high Q^2 pQCD requires we resum the contributions of $\alpha_S \log(Q^2/Q_0^2)$ terms. This yields the well documented DGLAP equations. As centre of mass energy $\sqrt{s}$, increases at moderate Q^2, we can technically encounter a second large logarithm, this time in $1/x \sim s/Q^2$. Resummation of this type leads to the celebrated Balitskij-Fadin-Kuraev-Lipatov (BFKL) equation for the gluon. The BFKL equation corresponds to ladder diagrams with (reggeized) gluon exchange along the chain.

One of the main predictions of the BFKL formalism is singular power law small x behaviour, $x^{-\lambda}$, of deep inelastic scattering. The exponent λ has been calculated at leading order [1, 2] and next-to-leading order [3, 4, 5] which contributes large negative corrections to the LO value. The leading order approximation of the BFKL equation should therefore be regarded as unreliable. It should be emphasised that the subleading $\log(1/x)$ effects are so strong that their next-to-leading (NLO) approximation alone is entirely unreliable already for reasonably small, yet relevant values, of the strong coupling, that is for $\alpha_S > 0.15$. The exact form of the sub-leading contribution, resummed to all orders, is unfortunately unknown. It may however be possible to pin down the dominant non-leading effects of well-defined physical origin, and to perform their exact resummation (that is going beyond the unreliable next-to-leading approximation) [5, 6]. In ref. [6] we have identified one class of such sub-leading corrections which followed from imposing a certain kinematical consistency constraint on the available phase space of the emitted gluons along the chain. At the next-to-leading level this constraint exhausts about 70% of the corrections to the BFKL exponent λ and, more important, the effects of this constraint can be resummed to all orders. After including the constraint in the (LO) BFKL equation, we obtain a formalism which makes it possible to implement the dominant subleading effects and to resum them to all orders. In ref. [7] the BFKL equation supplemented by the consistency constraint was used in a quantitative analysis of the structure function F_2 within a unified BFKL and DGLAP scheme. In this paper we wish to study the effects of these modifications on the properties of final state processes in deep inelastic scattering (DIS), which are particularly sensitive on BFKL dynamics. These are DIS accompanied by a forward jet [8] and the associated process of DIS with forward π^0's [9]. The existing calculations of these processes have been performed within a LO BFKL framework, and it is clearly essential to improve the analysis by incorporating the effects of the above constraint.

The DIS + forward jet measurement first proposed by Mueller [8] can be a very useful tool for probing the BFKL dynamics where the diffusion of the transverse momentum along the gluon chain plays an important role. By choosing the configuration in which $k_{jT}^2 \sim Q^2$, where k_{jT}^2 denotes the jet transverse momentum, we eliminate the phase space region of strongly-ordered transverse momenta of the gluons along the chain, i.e. the region $k_{jT}^2 \ll k_1^2 ... \ll k_n^2 \ll Q^2$, which is the dominant factor driving the increase of F_2 in the double leading log approximation. Moreover in the forward configuration $x_j^p \gg x$, where x is the Bjorken parameter, we have large subenergy available for jet production that justifies the use of BFKL dynamics.

We can also study DIS + forward π^0's [9]. This is a more refined version of the DIS + forward jet case, in the sense that we no longer have potential ambiguities derived from hadronisation effects or jet finding algorithms. The distinguishing features are discussed more fully in section 5.

We first motivate higher order constraints which should naturally be implemented in a BFKL formalism. We then show how observables for DIS + forward jet/π^0 can be calculated from the unintegrated gluon distribution, evolved from the virtual photon end of the BFKL ladder [1] , unlike the hybrid evolution used in ref. [9]. It is more convienient to impose the higher order constraints in the present form of the evolution. We then compare our calculations with experimental results for DIS + forward jet production from H1 [10] and ZEUS [11], and show a comparison of our analysis with very recent results for π^0 cross-sections obtained by the H1 collaboration at HERA [12]. Finally we estimate the cross-section for production of two jets satisfying the forward criteria.

2 The unintegrated BFKL gluon from $\gamma^* g$ fusion

In this section we shall describe the formalism needed for the theoretical description of the DIS + forward jet measurement based on the BFKL equation [13]. The natural quantity driving physi-

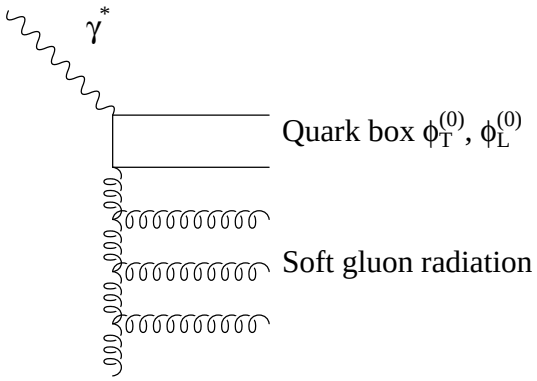

Figure 1: Diagram showing the $\gamma^* g$ fusion, including the soft gluon radiation ladder.

cal processes in DIS in the small Bjorken-x region of (x, Q^2) phase-space is the *unintegrated gluon distribution*, ϕ_i

$$x_g^\gamma g_i(x_g^\gamma, Q^2, \bar{Q^2}) = \int^{\bar{Q^2}} \frac{dk_T^2}{k_T^2} \phi_i(x_g^\gamma, k_T^2, Q^2), \tag{1}$$

where $g_i(x_g^\gamma, Q^2, \bar{Q^2})$ are the conventional gluon distributions of a photon of virtuality Q^2 and polarisation $i = T, L$, probed at a scale $\bar{Q^2}$. The parameter x_g^γ denotes the longitudinal momentum fraction of the parent virtual photon carried by the gluon and k_T denotes its transverse momentum. The gluon four momentum k has the following Sudakov decomposition

$$k = -x_g^p p + x_g^\gamma q' + \boldsymbol{k_T}, \tag{2}$$

[1] The present form of analysis in which we iterate from the virtual photon will facilitate comparison with the analysis of forward jet production in terms of the partonic structure of the virtual photon.

where p is the four momentum of the nucleon, and the light-like vector q' is defined by

$$q' = q + xp. \tag{3}$$

The variable x is the Bjorken parameter conventionally defined as $x = Q^2/(2p.q)$ and, as usual, $Q^2 = -q^2$ with q being the four momentum carried by the virtual photon.

The contribution to ϕ arising from the virtual photon can be thought of in terms of virtual photon-gluon fusion through a *quark-box* coupled to an equation describing the subsequent evolution of the gluon distribution. The quark box driving terms, $\phi_T^{(0)}$ and $\phi_L^{(0)}$, can be evaluated perturbatively

$$\phi_T^{(0)}(x_g^\gamma, k_T^2, Q^2) =$$

$$\sum_q e_q^2 \frac{\alpha_S}{4\pi^2} Q^2 \int_{x_g^\gamma}^1 d\beta \int d^2\boldsymbol{\kappa_T} \left\{ \left[\beta^2 + (1-\beta)^2\right] \left(\frac{\boldsymbol{\kappa_T}}{D_1} - \frac{(\boldsymbol{\kappa_T} - \boldsymbol{k_T})}{D_2} \right)^2 + m_q^2 \left(\frac{1}{D_1} - \frac{1}{D_2} \right)^2 \right\}, \tag{4}$$

$$\phi_L^{(0)}(x_g^\gamma, k_T^2, Q^2) = \sum_q e_q^2 \frac{\alpha_S}{\pi^2} Q^2 \int_{x_g^\gamma}^1 d\beta \int d^2\boldsymbol{\kappa_T} \beta^2 (1-\beta)^2 \left(\frac{1}{D_1} - \frac{1}{D_2} \right)^2$$

where the denominator functions are

$$D_1 = \kappa_T^2 + \beta(1-\beta)Q^2 + m_q^2,$$

$$D_2 = (\boldsymbol{\kappa_T} - \boldsymbol{k_T})^2 + \beta(1-\beta)Q^2 + m_q^2.$$

The quark mass m_q is set to zero for the light u, d, and s quarks and taken to be 1.4GeV for the charm quark. Taking these driving terms we then evolve the unintegrated gluon distributions, ϕ_T and ϕ_L, using the BFKL equation from the virtual photon end of the BFKL ladder

$$\phi_i(x_g^\gamma, k_T^2, Q^2) = \phi_i^{(0)}(x_g^\gamma, k_T^2, Q^2) +$$

$$\bar{\alpha_S}(k_T^2) k_T^2 \int_{x_g^\gamma}^1 \frac{dz}{z} \int_{k_0^2}^\infty \frac{dk_T'^2}{k_T'^2} \left\{ \frac{\phi_i(x_g^\gamma/z, k_T'^2, Q^2) - \phi_i(x_g^\gamma/z, k_T^2, Q^2)}{|\, k_T^2 - k_T'^2 \,|} + \frac{\phi_i(x_g^\gamma/z, k_T^2, Q^2)}{(4k_T'^4 + k_T^4)^{\frac{1}{2}}} \right\}, \tag{5}$$

where $i = T$ or L, $\bar{\alpha_S} = 3\alpha_S/\pi$, and x_g^γ is the fraction of the virtual photon's longitudinal momentum carried by the gluon. We will show results for infrared cut-off k_0^2 varied within the range $0.5 - 1\text{GeV}^2$.

We require strong ordering in $(x_g^\gamma)_i$ along the gluon chain

$$(x_g^\gamma) \ll (x_g^\gamma)_1 \ll ... \ll (x_g^\gamma)_n.$$

The present approach differs from our earlier work [9] in that we no longer have a free parameter z_0 which specifies the end of the BFKL evolution. In our previous treatment [9] we performed a hybrid evolution of the gluon ladder in the sense that, while we allowed the k_T^2 diffusion from the quark box, the longitudinal momentum fractions were defined with respect to the proton end of the ladder and strongly ordered along the gluon chain. In that case z_0 was adjusted to give the correct normalisation for the DIS + jet data. In the present calculation the normalisation is, in principle, fixed by the theory. However, in practice, there is freedom due to the choice of the value of QCD scale, which we will quantify later. In summary, the present description of the behaviour of the quark-box gluon chain system can be considered as a calculation of the unintegrated gluon content of the virtual photon.

3 Higher order corrections

Calculations [3, 4, 5] have shown that the NLO corrections to the BFKL equation are large. This casts doubt upon the quantitative predictive power of any LO BFKL approach to small x DIS dynamics. Clearly, for phenomenological purposes, a method of including the higher order effects should be considered. One origin of subleading effects, which contributes to all orders, is the so called *consistency constraint* (CC) [6]. This requires that the virtuality of the emitted gluons along the chain should arise predominantly from the transverse components of momentum, in order for the small x (small x_g^γ) approximation to be valid, that is

$$q_T^2 < \frac{k_T^2}{z}, \tag{6}$$

where we have omitted a factor of $(1-z)$.

We can motivate the inclusion of the consistency constraint in the analysis by reference to the exponent λ governing small x behaviour, $x^{-\lambda}$. It has been shown [6] that by truncating the all order BFKL + CC solution at NLO, one recovers some 70% of the full, explicit NLO calculation in the effective exponent. It looks reasonable to suppose that this comprises the dominant part of all higher order effects.

Another physical source of sub-leading contributions comes from the imposition of the conservation of energy-momentum in multigluon emission. Such an effect has been investigated in ref. [14]. It turns out that the consistency constraint subsumes energy-momentum conservation over a wide region of the allowed phase space [6].

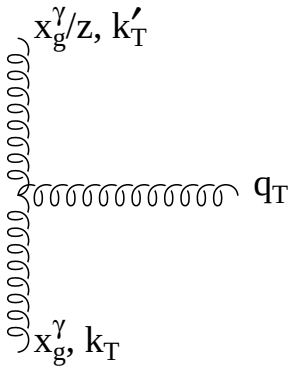

Figure 2: Diagram to illustrate the radiation of soft gluons from the reggeized gluonic propagator in the t-channel.

The CC places restrictions on the available phase space under the integration in the BFKL equation (5). This manifests itself as a Θ-function multiplying the kernel component governing real gluon emissions. Upon implementing this, we obtain a modified BFKL equation

$$\phi_i(x_g^\gamma, k_T^2, Q^2) = \phi_i^{(0)}(x_g^\gamma, k_T^2, Q^2) +$$
$$\bar{\alpha_S} k_T^2 \int_{x_g^\gamma}^1 \frac{dz}{z} \int_{k_0^2}^\infty \frac{dk_T'^2}{k_T'^2} \left\{ \frac{\Theta\left(k_T^2/k_T'^2 - z\right) \phi_i(x_g^\gamma/z, k_T'^2, Q^2) - \phi_i(x_g^\gamma/z, k_T^2, Q^2)}{\mid k_T^2 - k_T'^2 \mid} + \frac{\phi_i(x_g^\gamma/z, k_T^2, Q^2)}{(4k_T'^4 + k_T^4)^{\frac{1}{2}}} \right\}. \tag{7}$$

4 Forward jet production in DIS.

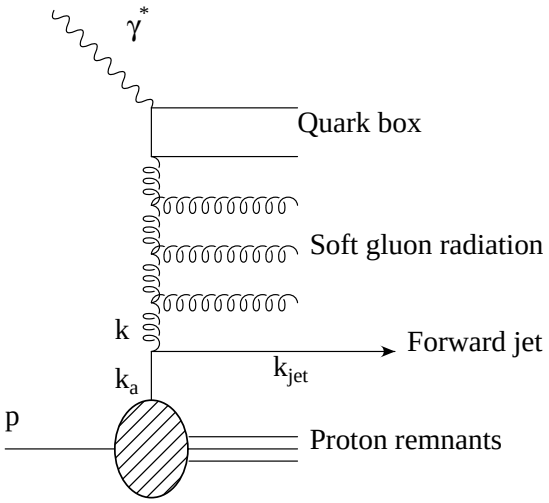

Figure 3: Diagram showing forward jet production driven by $\gamma^* g$ fusion coupled to evolution through a BFKL-type ladder. The struck parton from the proton could in principle be either a gluon or a quark.

Given that measurements of F_2 proved unable to unambiguously determine small x dynamics, less inclusive alternative approaches were needed. One such process is Mueller's proposal [8]:

$$\gamma^* + p \longrightarrow \text{jet} + X$$

According to Mueller, DIS events containing an identified forward jet provide a particularly clean window on small x dynamics. By requiring that $Q^2 \simeq k_{jT}^2$ we ensure minimal DGLAP type evolution, and any remaining features must be the result of dynamics from the small x limiting region of the (x, Q^2) phase-space. Moreover by considering jets with large fractions of the proton's longitudinal momentum, x_j^p allowing x/x_j^p to be as small as possible, on the one hand, will allow the use of BFKL dynamics, while on the other hand, involve parton distributions at values of x_j^p where they are well known.

4.1 QCD prediction for DIS + forward jet

The kinematics are such that we may use *strong ordering* at the parton-gluon-jet vertex

$$k_{aT}^2 \ll k_{jT}^2, \quad x_j^p \gg x,$$

where the Sudakov decomposition of the jet four momentum in terms of light-like momenta p and q' in analogy to (2) is

$$k_j = x_j^p p + x_j^\gamma q' + \boldsymbol{k_{jT}}. \tag{8}$$

We can relate the longitudinal momentum fractions at the jet vertex through strong-ordering and the jet on-shell condition, $k_j^2 = 0$. This allows us to deduce that

$$2x_j^p x_j^\gamma (p.q') = k_{jT}^2,$$

$$x_g^\gamma \simeq x_j^\gamma = \frac{k_{jT}^2}{2x_j^p(p.q)} = \frac{k_{jT}^2 x}{Q^2 x_j^p}.$$

Using the prescription described in the previous section, we solve numerically for ϕ in the modified BFKL equation, via an expansion in Chebyshev polynomials, and finally determine the unintegrated gluon distribution

$$\Phi_i(\frac{x}{x_j^p}, k_{jT}^2, Q^2) \;=\; \phi_i(x_g^\gamma = \frac{k_{jT}^2 x}{Q^2 x_j^p}, k_{jT}^2, Q^2). \tag{9}$$

$\Phi_i(x/x_j^p, k_{jT}^2, Q^2)$ can then be used to calculate the differential structure functions that drive the forward jet process through

$$\frac{\partial^2 F_i}{\partial x_j^p \partial k_{jT}^2} = \frac{3\alpha_S}{\pi k_{jT}^4}\left(\sum_a f_a(x_j^p, k_{jT}^2)\right)\Phi_i\left(\frac{x}{x_j^p}, k_{jT}^2, Q^2\right), \tag{10}$$

where $\sum_a f_a$ is the sum over parton distributions assuming t-channel pole dominance.

$$\sum_a f_a = g + \frac{4}{9}\sum_q (q + \bar{q}). \tag{11}$$

These quantities can be substituted into an expression for the differential cross-section for forward jets

$$\frac{\partial \sigma_j}{\partial x \partial Q^2 \partial x_j^p \partial k_{jT}^2} = \frac{4\pi\alpha^2}{xQ^4}\left[(1-y)\frac{\partial^2 F_2}{\partial x_j^p \partial k_{jT}^2} + \frac{1}{2}y^2 \frac{\partial^2 F_T}{\partial x_j^p \partial k_{jT}^2}\right], \tag{12}$$

where $y = (p.q)/(p_e.q)$ and $F_2 = F_T + F_L$.

4.2 Comparison with HERA data

Finally we are in a position to be able to confront our calculation with the HERA data. We numerically integrate the differential cross-section over the kinematic regions used by the H1 [10] and ZEUS [11] collaborations, see Table 1. The results are shown in Fig.4. Since the parton distributions (11) are required in a kinematic domain where they are well known the results are not sensitive to the particular set that is used. However there is a dependence of the results on the QCD scale. To be consistent we use a recent *leading order* set of partons. We take the LO set from [15], for which $\Lambda(\mathrm{QCD}) = 0.174\mathrm{GeV}$ for four flavours. The three curves in the figure correspond to the arguments of α_S in (4) and (10) and the infrared cut-off in (7) being respectively taken to be [2]

$$\begin{array}{lcccl} \text{(i)} & (k_T^2 + m_q^2)/4, & k_T^2/4, & k_0^2 = 0.5\mathrm{GeV}^2 & \text{(upper dashed)} \\ \text{(ii)} & (k_T^2 + m_q^2)/4, & k_T^2/4, & k_0^2 = 1\mathrm{GeV}^2 & \text{(continuous)} \\ \text{(iii)} & (k_T^2 + m_q^2), & k_T^2, & k_0^2 = 0.5\mathrm{GeV}^2 & \text{(lower dashed).} \end{array} \tag{13}$$

The sensitivity to the choice of scales for α_S is therefore seen by comparing the predictions for (i) and (iii), and the sensitivity to the value chosen for the infrared cut-off k_0^2 by comparing (i) and (ii). We see that the uncertainty due to k_0^2 is much less than the uncertainty due to the choice of scales. From Fig. 4 we see that the shape of the x distributions of the DIS + forward jet data are modelled well. Moreover the predicted normalisation is satisfactory in that agreement exists for a physically reasonable choice of scales and of the infrared cut-off k_0^2. The experimental data correspond to the measurements at the hadron level. The hadronisation effects can lower the cross-section by about 15-20%. We comment on the comparison with data further in section 7.

[2] When the scale of α_S is less than k_0^2, in choices (i) and (ii), we freeze the coupling at $\alpha_S(k_0^2)$.

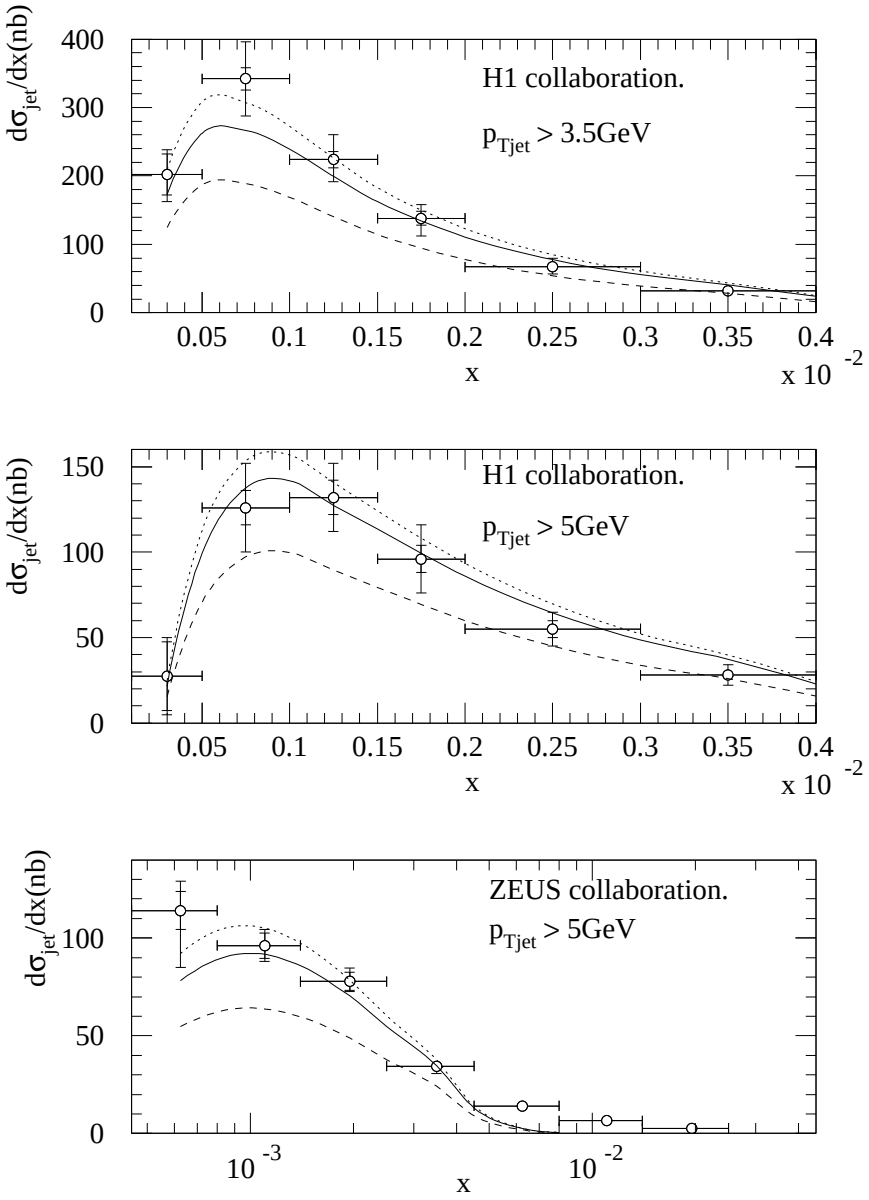

Figure 4: The DIS + forward jet differential cross-section versus Bjorken-x as measured at the hadron level by the H1 [10] and ZEUS [11] collaborations. The kinematic cuts are given in Table 1. The curves are predictions at the parton level, based on the BFKL formalism including sub-leading corrections, corresponding to the three choices of scales and infrared cut-off given in (13) .

H1 cuts	ZEUS cuts
$E'_e > 11\text{GeV}$	$E'_e > 10\text{GeV}$
$y_e > 0.1$	$y_e > 0.1$
$x_j^p > 0.035$	$x_j^p > 0.036$
$k_{jT} > 3.5\text{GeV}$	$E_{jT} > 5\text{GeV}$
$0.5 < k_{jT}^2/Q^2 < 2$	$0.5 < E_{jT}^2/Q^2 < 2$
$7^o < \theta_{jet} < 20^o$	$\eta_{jet} < 2.6$
$160^o < \theta_e < 173^o$	

Table 1: Table showing the kinematic restrictions imposed on DIS events at HERA for forward jet production.

5 DIS events containing a forward π^0

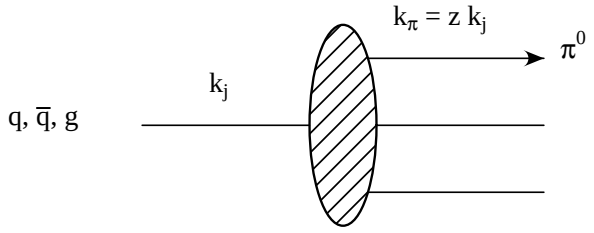

Figure 5: Schematic showing collinear fragmentation of a forward parton jet of momentum k_j into a forward pion of momentum zk_π. The process is described by fragmentation functions, $D_i(z, \mu^2)$

A complementary reaction to Mueller's forward jet process is provided by the production of forward π^0 mesons in deep inelastic events [9]. The driving process here is the same as before, with $\gamma^* g$ fusion coupled to BFKL-type gluon evolution, ejecting a parton within the proton as a forward jet. However, we now allow the parton to evolve into a shower of particles containing a pion collinear to the initial parton jet

$$\gamma^* + p \longrightarrow \pi^0 + X.$$

There are advantages in attempting to measure the forward π^0 cross-section as compared to the parent forward-jet cross-section.

- Experimentally one can more unambiguously identify a forward π^0 than a jet.
- By measuring π^0's at relatively low $x_\pi, p_{T\pi}$ we effectively collect data for energetic forward jets with $x_j > x_\pi$ and $k_{jT} > p_{T\pi}$, which might otherwise go undetected.
- Another consequence of looking for a specific final state is that we eliminate our dependence on jet-finding algorithms. We can unambiguously determine the signal due to the measurement of a real π^0 instead of worrying about jet definitions.
- Finally, we eliminate hadronisation uncertainties. All non-perturbative hadronisation effects are swept into the fitted parametrisations of the fragmentation functions.

On the other hand, by requiring a single energetic fragment of the jet we reduce the cross-section.

5.1 Including forward jet $\to \pi^0$ fragmentation

We use the LO $\pi^{\pm}$ fragmentation functions of Binnewies et al. [16]. They present results of the form

$$D_i(z,\mu^2) = N_i(\mu^2) z^{\alpha_i(\mu^2)} (1-z)^{\beta_i(\mu^2)} \tag{14}$$

where $i = g, q, \bar{q}$ and μ^2 is the fragmentation scale. Here we take the fragmentation scale simply as k_{jT}^2. The functions for π^0 are taken to be $\frac{1}{2}(\pi^+ + \pi^-)$ distributions

The form of the fragmentation requires the π^0 to carry $z = x_\pi / x_j^p$ of the jet's longitudinal momentum, in a direction collinear with the initial parton. With this assumption we can relate the transverse momentum of the π^0 and the forward jet

$$\boldsymbol{k_{\pi T}} = z\boldsymbol{k_{jT}}.$$

Next we obtain the cross-section for π^0 production by convoluting the DIS + forward jet cross-section (12) with the π^0 fragmentation parametrisations (14) [9]

$$\frac{\partial\sigma_{\pi^0}}{\partial x_\pi \partial p_{T\pi}^2 \partial x \partial Q^2} = \int_{x_\pi}^1 dz \int dx_j^p \int dk_{jT}^2 \delta(x_\pi - z x_j^p) \delta(p_{T\pi} - z k_{jT})$$

$$\left\{ \frac{\partial\sigma_g}{\partial x_j^p \partial k_{jT}^2 \partial x \partial Q^2} D_g^{\pi^0}(z, k_{jT}^2) + \frac{4}{9} \sum_q \left[\frac{\partial\sigma_q}{\partial x_j^p \partial k_{jT}^2 \partial x \partial Q^2} D_q^{\pi^0}(z, k_{jT}^2) + \frac{\partial\sigma_{\bar{q}}}{\partial x_j^p \partial k_{jT}^2 \partial x \partial Q^2} D_{\bar{q}}^{\pi^0}(z, k_{jT}^2) \right] \right\}. \tag{15}$$

The differential cross-sections on the right-hand-side, $\partial\sigma_j / \partial x_j^p \partial k_{jT}^2 \partial x \partial Q^2$ with $j = q, \bar{q}, g$, are given by (10) and (12) with the replacement of $\sum f_a$ by $f_q, f_{\bar{q}}$ and f_g respectively.

5.2 Comparison with forward π^0 data

There exist two sets of measurement of deep inelastic events containing forward π^0 mesons. First there are the 1994 H1 data [10], and now the recent analysis of the 1996 H1 data [12]. The kinematic cuts used to obtain these data samples are summarized in Table 2. The π^0 spectra are defined through

$$\frac{1}{N}\frac{dn_\pi}{dx} = \frac{1}{\sigma_{tot}}\frac{\partial\sigma_\pi}{\partial x} \tag{16}$$

where n_π is the number of π^0's, and N is the total number of DIS events. The recent H1 results [12] are fully comprehensive, with histograms showing the differential cross-section for π^0 production as functions of x, Q^2, $p_{T\pi}$ and η_π. We compute the π^0 cross-section using exactly the same three choices of the scales of α_S and infrared cut-off k_0^2 as we used for the DIS + forward jet predictions, see Section 4.2.

In Fig. 6 we compare our analysis with the 1994 H1 π^0 spectra in three x_π regimes. We find a satisfactory description of the shape, and that the normalisation is best described by choice (iii) of the scales of (13). The factor of two overshoot of the data by the previous predictions [9] is gone. The reason is the suppresion due to the inclusion of the sub-leading corrections. In Figures 7 through 10 we compare our calculations of the π^0 differential cross-sections as a function of x, Q^2, $p_{T\pi}$ and η_π, with the new H1 data [12]. As in the DIS + forward jet process, we see that there is good overall agreement between the predictions and the DIS + forward π^0 data.

1994 H1 data	New H1 data
$E'_e > 12$GeV	
$y_e > 0.1$	$0.6 > y_e > 0.1$
$x_\pi > 0.01$	$x_\pi > 0.01$
$p_{T\pi} > 1$GeV	$p_{T\pi} > 2.5$GeV
$5^o < \theta_\pi < 25^o$	$5^o < \theta_\pi < 25^o$
$156^o < \theta_e < 173^o$	
	$2 < Q^2 < 70\text{GeV}^2$

Table 2: Table showing the kinematic restrictions imposed on DIS events by the H1 collaboration for forward π^0 production. For the 1996 data, implicit bounds are imposed on θ_e and E'_e by the y_e restriction.

The continuous curves, which are the set which best describe the forward jet data, are on average some 20% above the forward π^0 data. However the overall agreement is well within the theoretical and experimental uncertainties. (Note that no allowance has been made for the uncertainty in the fragmentation functions for the pion). Moreover note that the jet data are shown at the hadron level. If we were to correct for hadronisation effects, then the parton level jet data are expected to be 15-20% lower [17], and the overall consistency of the QCD description is even better than shown.

If we look at the description of the forward π^0 data in more detail then we see, from Figs. 7 and 9, that the Q^2 behaviour of the DIS + forward π^0 data is not reproduced in detail by any single one of the three sets of predictions. For instance for $Q^2 < 4.5\text{GeV}^2$ the continuous curve is below the data, although in agreement within the errors, whereas for $Q^2 > 4.5\text{GeV}^2$ the curve is above the data by about two standard deviations on average. Note that the relative Q^2 behaviour evident between Figs. 7(b,c,d) simply reflects the comparison of the curves with the data in Fig. 9(a). However, it is worth repeating that the overall agreement between the predictions of small x dynamics and the DIS + π^0 data is much improved since the previous comparison [9]. We comment further on the predictions in Section 7.

6 Forward dijet production

Forward dijet production provides a further complementary measure of small x dynamics [18]

$$\gamma^* + p \longrightarrow \text{jet}_1 + \text{jet}_2 + X$$

The additional second jet is then required to fulfil the same forward experimental cuts as for the simple jet data. The process is shown in Fig. 11. We may neglect the effects of soft gluon radiation in the rapidity gap, as the experimental constraints are too restrictive to allow significant development of a second chain of gluon emission between the jets [18]

$$x_{j2} \lesssim x_{j1} \sim O(1).$$

Analogously to the single forward jet case, the dijet cross-section is determined by

$$\frac{\partial\sigma}{\partial x \partial Q^2 \partial x_{j1} \partial k^2_{jT1} \partial x_{j2} \partial k^2_{jT2}} = \frac{4\pi\alpha^2}{xQ^4}\left[(1-y)\frac{\partial F_2}{\partial x_{j1} \partial k^2_{jT1} \partial x_{j2} \partial k^2_{jT2}} + \frac{1}{2}y^2 \frac{\partial F_T}{\partial x_{j1} \partial k^2_{jT1} \partial x_{j2} \partial k^2_{jT2}}\right],$$

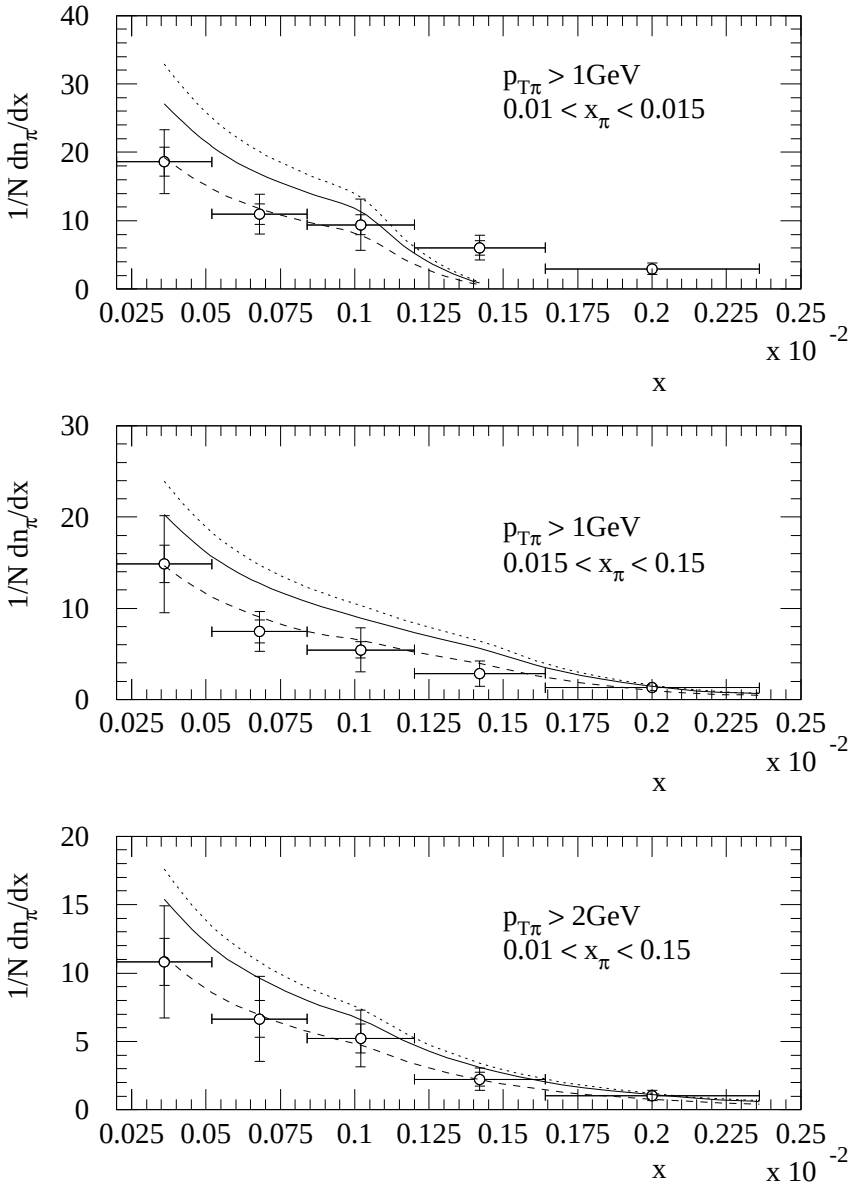

Figure 6: The π^0 spectra (16) versus Bjorken-x obtained from 1994 H1 data [10]. The curves are predictions, based on the BFKL formalism including sub-leading corrections, corresponding to the three choices of scales and infrared cut-off given in (13). [The restriction $x/x_\pi < 0.1$ limits the comparison to the domain $x \lesssim 10^{-3}$ in the upper plot.]

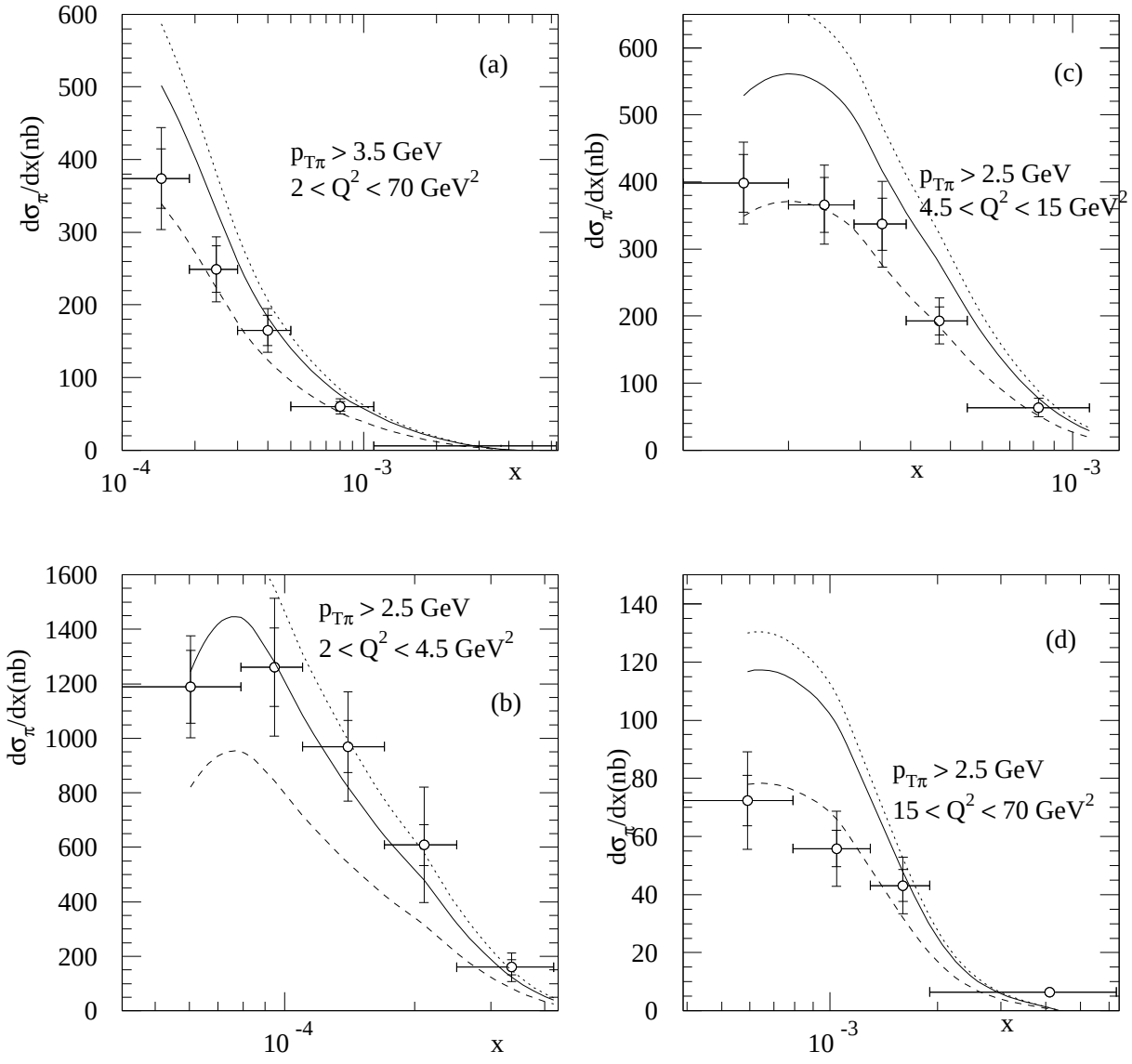

Figure 7: The π^0 differential cross-section versus Bjorken-x obtained from 1996 H1 (preliminary) data [12]. The curves are predictions, based on the BFKL formalism including sub-leading corrections, corresponding to the three choices of scales and infrared cut-off given in (13) .

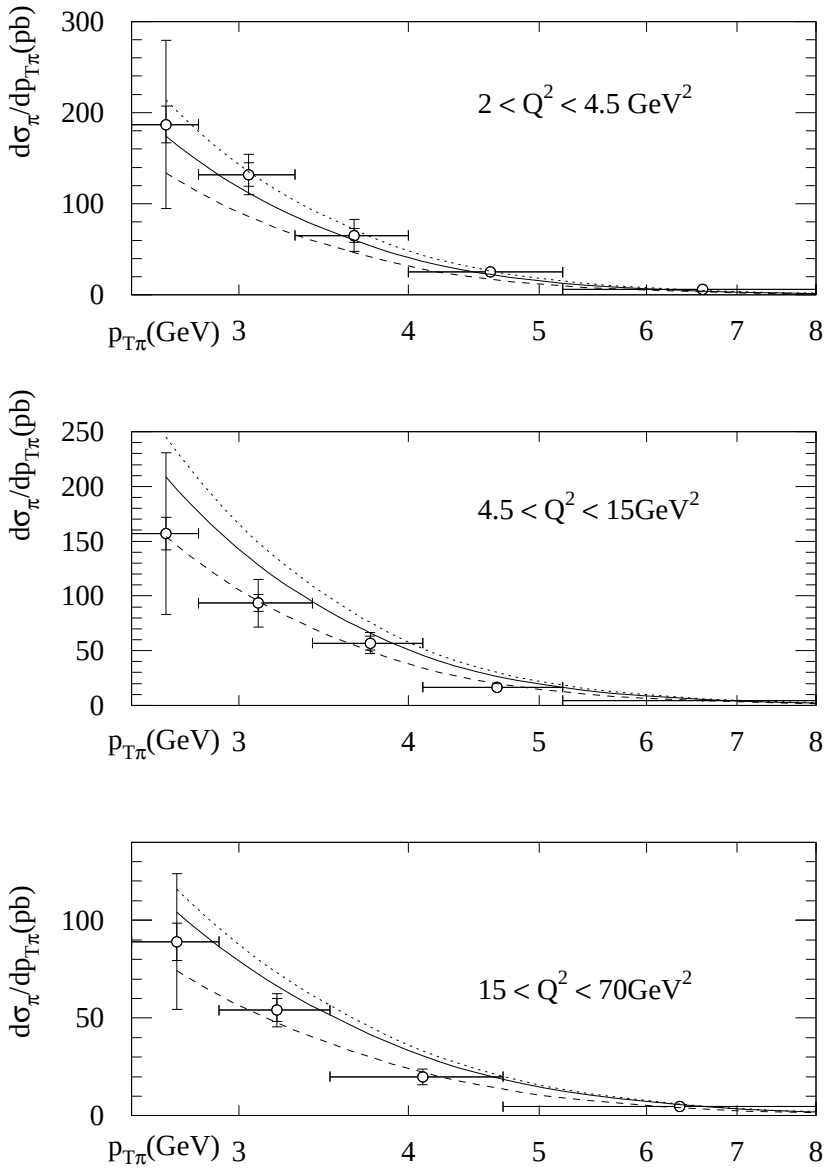

Figure 8: π^0 differential cross-section in transverse momentum, obtained from 1996 H1 (preliminary) data [12]. The curves are predictions, based on the BFKL formalism including sub-leading corrections, corresponding to the three choices of scales and infrared cut-off given in (13) .

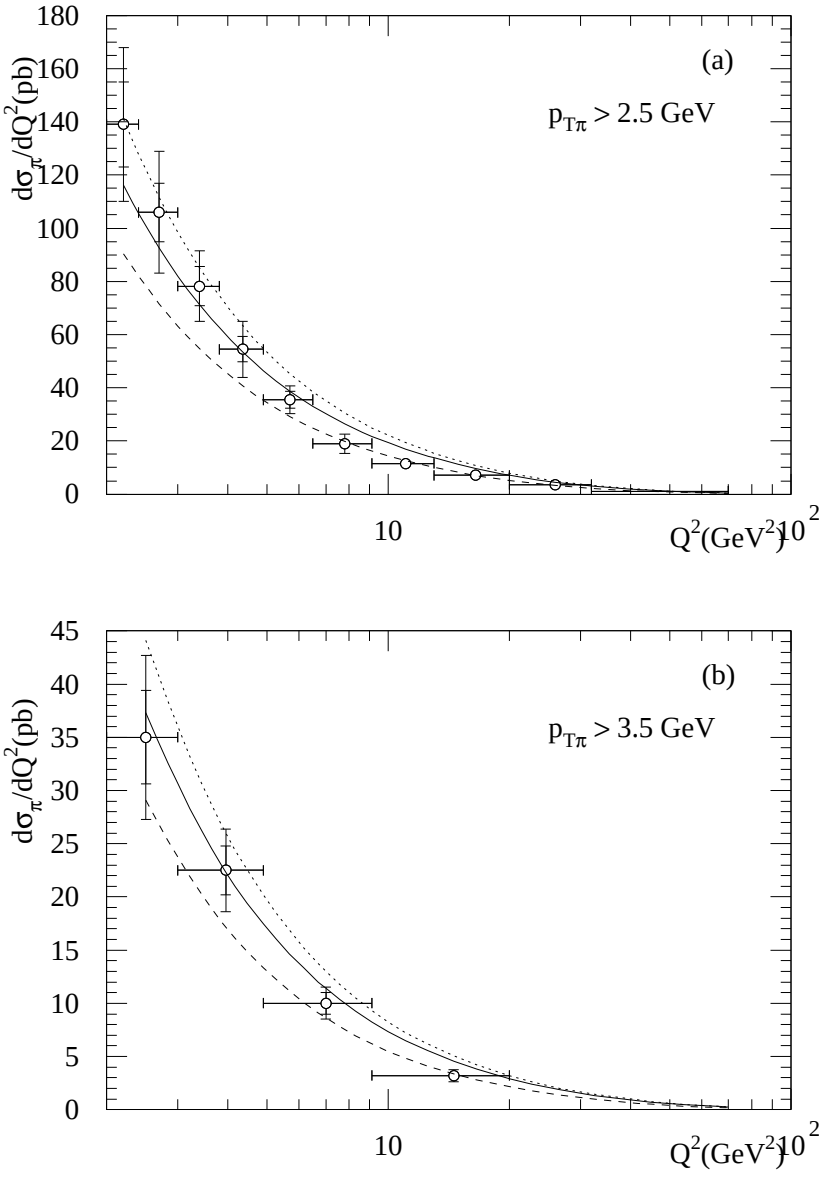

Figure 9: The π^0 differential cross-section versus Q^2 obtained from 1996 H1 (preliminary) data [12]. The curves are predictions, based on the BFKL formalism including sub-leading corrections, corresponding to the three choices of scales and infrared cut-off given in (13) .

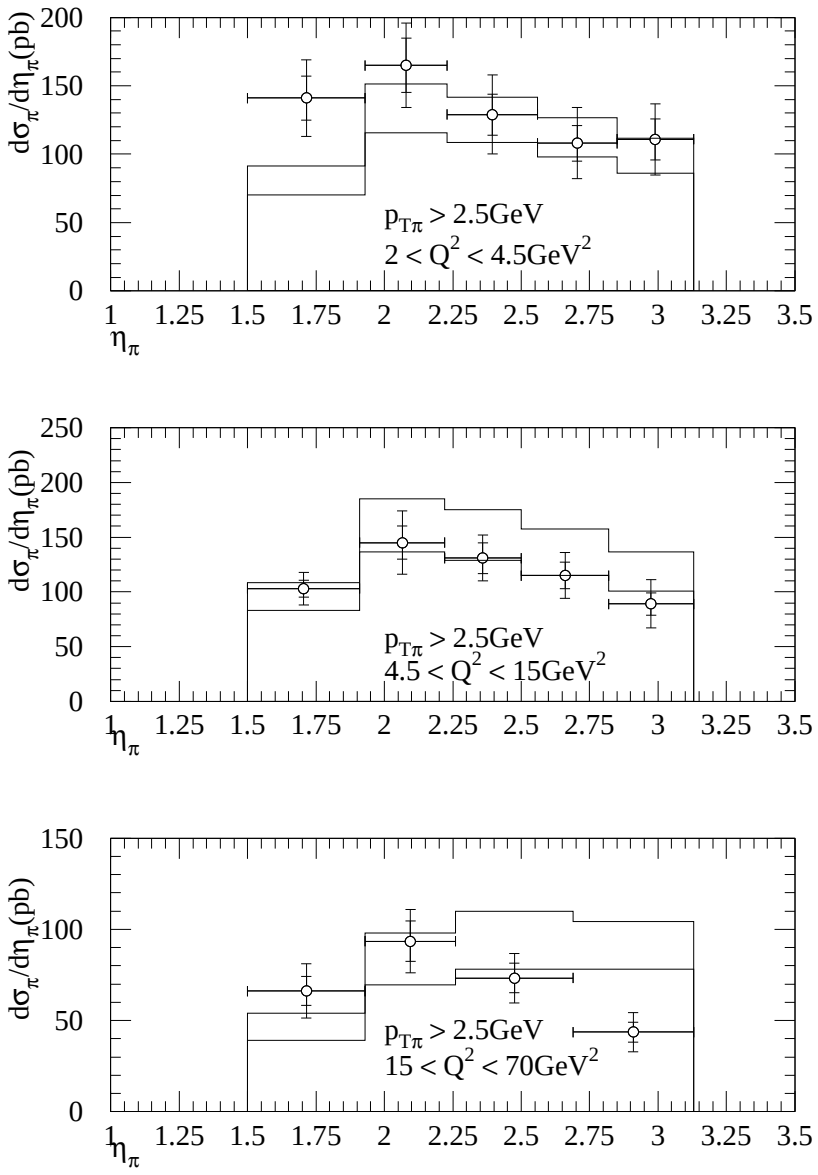

Figure 10: The π^0 differential cross-section versus rapidity obtained from 1996 H1 (preliminary) data [12]. The upper and lower histograms are the predictions of the BFKL formalism including subleading corrections respectively corresponding to choices (ii) and (iii) of the scales and k_0^2 given in (13) .

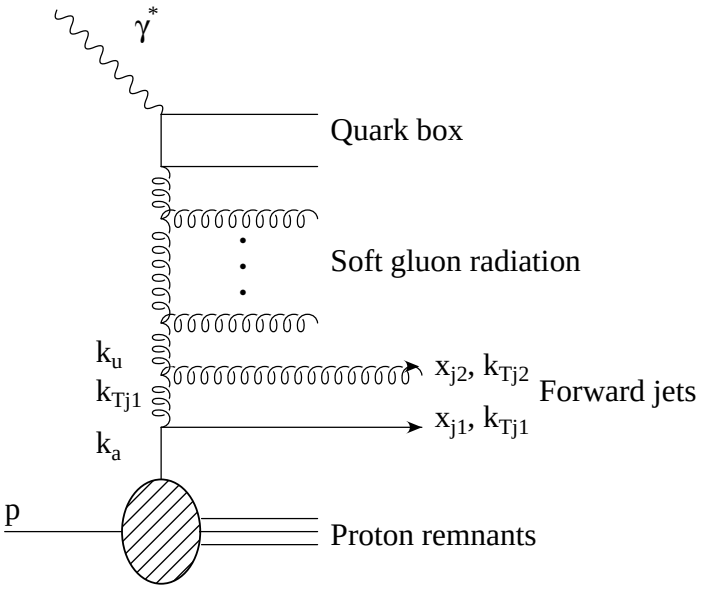

Figure 11: Diagram illustrating the emission of an extra forward jet in addition to the standard Mueller process.

(17)

with

$$x_{j2}\frac{\partial F_i}{\partial x_{j1}\partial k^2_{jT1}\partial x_{j2}\partial k^2_{jT2}} = \frac{1}{2\pi}\int_0^{2\pi} d\phi\Phi_i(x/x_{j2},k_u^2,Q^2)\frac{\bar{\alpha_S}\bar{\alpha_S}}{k_u^2 k^2_{jT2}k^2_{jT1}}\sum_a f_a(x_{j1},k^2_{jT1}). \qquad (18)$$

Here, ϕ is the azimuthal angular separation between the two forward jets, and k_u^2 is given by

$$k_u^2 = (\boldsymbol{k_{jT1}} + \boldsymbol{k_{jT2}})^2.$$

The azimuthal (ϕ) integration is performed numerically. Experimental jet resolution effects are included by imposing a cut, $R_{\rm min}$ in rapidity-azimuthal angle space:

$$\sqrt{(\Delta\eta)^2 + (\Delta\phi)^2} > R_{\rm min} = 1.$$

The H1 results published in 1994 quote a result of 6.0 ± 0.8 (stat) ± 3.2(syst) pb for the total cross-section of DIS + 2 forward jet events [10]. The calculation, including the consistency constraint, and imposing all the experimental cuts imposed by the H1 collaboration, results in a cross-section of $5.2, 4.8$ or 2.7pb depending on the different scales in α_S in (18) chosen as in (13) respectively. The predictions for the two-jet/one-jet ratio give $1.0, 1.1$ and 0.8% respectively, to be compared with the H1 measurement of $1.1 \pm 0.6\%$. That is, small x QCD is able to satisfactorily describe the observed rate of forward dijet production.

7 Discussion

The process of deep inelastic scattering (DIS) with a forward jet has quite a chequered history. The original "gold-plated" proposal of using DIS (x, Q^2) events containing a forward (x_j, k^2_{jT}) jet to study

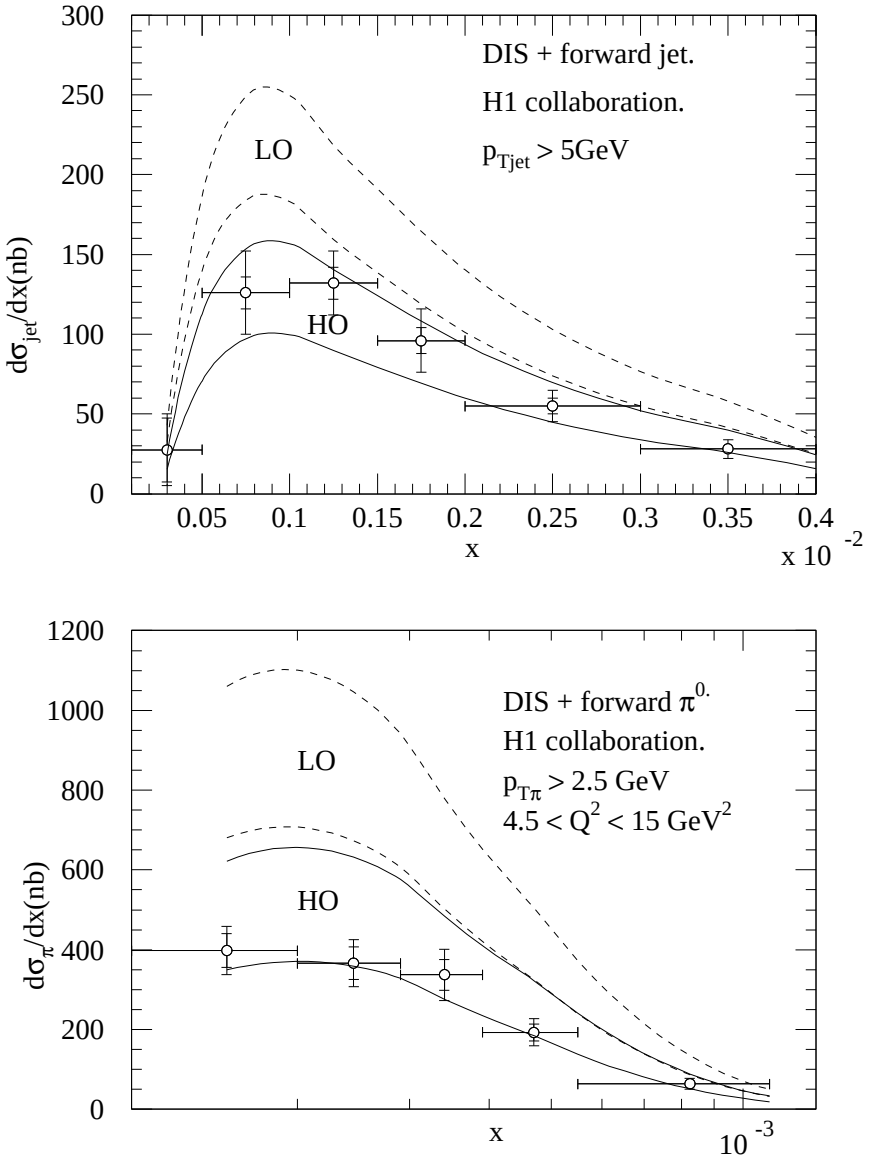

Figure 12: The differential cross-section for (a) DIS + forward jet, (b) DIS + forward π^0 (1996 H1 preliminary), events. The continuous and dashed curves correspond to the inclusion and omission of the consistency constraint. The lower curve of each pair corresponds to choosing the scales of α_S in (4) and (10) to be $k_T^2 + m_q^2$ and k_T^2 respectively. The upper curves have scales 1/4 of these values. In all cases the infrared cut-off in (7) is taken to be $k_0^2 = 0.5\text{GeV}^2$. The jet data are at the hadron level; converting to the parton level is expected to lower the jet data points by about 15-20% [17].

small x dynamics originally dates back to Mueller [8]. The idea was to study small x/x_j dynamics with $k_{jT}^2 \sim Q^2$ so that DGLAP effects are absent. The observation of a forward jet allows the deep inelastic scattering to take place off a parton (in a domain where the distribution $f_a(x_j, k_{Tj}^2)$ is well known) so that the small x/x_j dynamics can be studied free from the uncertainties in proton structure. The detailed formalism was provided soon after [13]. Then it was the turn of the experiments to collect a DIS + forward jet data sample. To obtain sufficient statistics, jets of relatively low k_{jT}^2 had to be considered, bringing problems of jet identification and measurement. On the theoretical side all phenmenological analyses [13, 19, 9] were based on the LO BFKL formalism, with a tendency of the predictions to overshoot the observed DIS + forward jet cross-section. At the same time it was also shown that one cannot obtain a sufficient increase of the cross-section, with decreasing x, from fixed order QCD calculations. In fact the fixed order (NLO) predictions are found to be a factor of 4 or more below the data [19, 20].

Recently a different approach [21, 22] to forward jet production has been proposed, based on describing the data in terms of the partonic structure of the virtual photon and DGLAP evolution. In this picture the dominant contribution in the region $Q^2 < k_{Tj}^2$ to the production of forward jets comes from the hard scattering of partons in the virtual photon with those in a proton. The calculations presented in ref. [22] are based on the parton distribution functions of the virtual photon evolved from some (low) scale Q_0^2 to the scale $\mu^2 = -\hat{t}$ (which is greater than k_{Tj}^2 but less than $k_{Tj}^2 + Q^2$). The parton distributions in virtual photons which are used in the estimates of the forward jet cross-sections were taken from ref. [23]. These parton distributions contain a rather arbitrary, although phenomenologically plausible, parameterization of the Q^2 dependence. At large Q^2, however, the parton distributions in the virtual photon are dominated by the point-like contribution which can be completely specified in perturbative QCD. In fact the approach developed in [21] is not very sensitive to the specific parameterisation of the parton distributions of the virtual photon. Our calculations based upon the BFKL equation may also be interpreted in terms of hard scattering of partons in a virtual photon. In this case, however, the Q^2 dependence of the parton distributions is not arbitrary, but rather is dynamically specified by the impact factor defined by the quark box. This impact factor corresponds to the point-like $\gamma^* q\bar{q}$ coupling. The analogy with the resolved photon picture becomes more evident if we approximate the BFKL evolution by its double leading logarithm approximation corresponding to strongly-ordered transverse momenta from Q^2 towards the hard scale k_{Tj}^2. The BFKL-based calculation should not therefore be interpreted as an alternative explanation to the resolved virtual photon picture since the latter is just part of the former. The BFKL description also has the merit of treating in a unified way all possible kinematical configurations. It does not in particular divide the underlying mechanism depending upon the relations between the potentially large scales (Q^2 and k_{Tj}^2) of the problem.

There have been two recent developments, both of which we have considered in this paper. First, DIS + forward π^0 process has also been measured. These data provide a complementary measurement which overcomes the experimental ambiguities inherent in the measurements of forward jets, albeit at the expense of a reduced rate. Second, as far as BFKL theory itself is concerned, there now exist complete NLO results available. These indicate that sub-leading effects are very important and cannot be neglected in a confrontation of small x dynamics with the data. In this paper we include subleading contributions in the description of DIS + forward jet and forward π^0 data. The effect of including the subleading terms can be seen from Fig. 12. We show the predictions for DIS + forward jet and DIS + forward π^0 with and without the consistency constraint included for two physically reasonable choices of scale. We see that the subleading terms (that is the consistency constraint) reduce the

predictions at the smaller values of x by almost a factor of two. There is a sizeable ambiguity in the predictions due to the choice of scale, but nevertheless both sets of data favour the inclusion of the sub-leading terms. Even though the subleading effect suppresses the cross-sections, the predictions remain sufficiently steep with decreasing x to describe the data. By inspecting the comparison shown in the two plots in Fig. 12 we note that, relative to the data, the DIS + forward π^0 predictions are lower than those for the DIS + jet process. However the comparison for the DIS + π^0 process is Q^2 dependent, see Fig. 9 and 7. On average the forward π^0 predictions are about 20% above the data if the scales are chosen so as to give an optimum description of the forward jet data. This discrepancy is well within the total uncertainties. Moreover, as was mentioned before, the experimental data on the forward jet cross-sections correspond to the measurements at the hadron level, while our theoretical predictions concern the parton level. The hadronisation effects are expected to raise the parton level jet cross-section by about 15-20% [17], and so the overall consistency between the forward jet and π^0 data and the small x QCD predictions shown at the parton level in Fig. 12, is in fact better than shown. Since we can identify and measure less energetic forward π^0's than jets, we are able to sample smaller values of x in the former process.

We conclude that there exists an economical, physically-based description of both the DIS + forward jet and the DIS + forward π^0 data in terms of the small x QCD framework.

Acknowledgements

We thank Franz Eisele, Thorsten Wengler, Ewelina Mroczko-Łobodzińska and Jesus Guillermo Contreras for their interest in this work and for information concerning the data. We thank Marco Stratmann and Mark Wüsthoff for useful discussions, and Bjorn Pötter for illuminating comments. JK thanks the Physics Department and Grey College of the University of Durham, and JJO thanks the Institute for Nuclear Physics of Krakow for their warm hospitalities. This work was supported in part by the UK Particle Physics and Astronomy Research Council, by the Polish State Committee for Scientific Research (grant no. 2 P03B 089 13) and by the EU Fourth Framework Programme TMR, Network 'QCD and Particle Structure' (contract FMRX-CT98-0194, DG12-MIHT).

References

[1] E.A. Kuraev, L.N. Lipatov and V.S. Fadin, *Sh. Eksp. Teor. Fiz.* **72** (1977) 373, (*Sov. Phys. JETP* **45** (1977) 199); Ya. Ya. Balitzkij and L.N. Lipatov, *Yad. Fiz.* **28** (1978) 1597, (*Sov. J. Nucl. Phys.* **28** (1978) 822); J.B. Bronzan and R.L. Sugar, *Phys. Rev.* **D17** (1978) 585; T. Jaroszewicz, *Acta. Phys. Polon.* **B11** (1980) 965.

[2] L.N. Lipatov, in "Perturbative QCD", edited by A.H. Mueller (World Scientific, Singapore 1989), p.441.

[3] V.S. Fadin, M.I. Kotskii and R. Fiore, *Phys. Lett.* **B359** (1995) 181; V.S. Fadin, M.I. Kotskii, L.N. Lipatov, hep-ph/9704267; V.S. Fadin, R. Fiore, A. Flachi and M.I. Kotskii, *Phys. Lett.* **B422** (1998) 287; V.S. Fadin and L.N. Lipatov, hep-ph/9802290; *Phys. Lett.* **B429** (1998) 127; V.S. Fadin, hep-ph/9807527, hep-ph/9807528; M. Ciafaloni and G. Camici, *Phys. Lett.* **B386** (1996) 341; **B412** (1997) 396; **B417** (1998) 390 (E); *Phys. Lett.* **B430** (1998) 349; M. Ciafaloni, hep-ph/9709390.

[4] D.A. Ross, *Phys. Lett.* **B431** (1998) 161.

[5] G.P. Salam, *JHEP* **9807** (1998) 019.

[6] J. Kwieciński, A.D. Martin and P.J. Sutton, *Z. Phys.* **C71**, 585 (1996).

[7] J. Kwieciński, A.D. Martin and A. Stasto, *Phys. Rev.* **D56** (1997) 3991.

[8] A. Mueller, *Nucl. Phys.* **B** (*Proc. Suppl*) **18C** (1990) 125; *J. Phys.* **G17**, 1443 (1991).

[9] J. Kwieciński, S.C. Lang and A.D. Martin, *Eur. Phys. J.* **C6** (1999) 671.

[10] H1 Collaboration, C. Adloff et al., *Nucl. Phys.* **B538** (1999) 3.

[11] ZEUS Collaboration, *Eur. Phys. J.* **C6** (1999) 239.

[12] E. Elsen, talk given at the Physics Research Committee at DESY, Hamburg, January 13th 1999. See also Thorsten Wengler, Ph.D. Thesis, University of Heidelberg, DESY-THESIS-1999-011, January 1999.

[13] J. Bartels, A. De Roeck and M. Loewe, *Z. Phys.* **C54**, 635 (1992); J. Kwieciński, A.D. Martin and P.J. Sutton, *Phys. Rev.* **D46** (1992) 921; W.K. Tang, *Phys. Lett.* **B278** (1992) 363.

[14] L. H. Orr and W. J. Stirling, Contribution to ICHEP 98, Vancouver, July 1998, hep-ph/9811423.

[15] A.D. Martin, R.G. Roberts, W.J. Stirling and R.S. Thorne, *Phys. Lett.* **B443** (1998) 301.

[16] J. Binnewies, B.A. Kniehl and G. Kramer, *Phys. Rev.* **D52** (1995) 4947.

[17] M. Wobisch, talk given at Workshop on DIS and QCD (DIS'97), Chicago, April 1997; T. Wengler, Private communication.

[18] J. Kwieciński, C.A.M. Lewis and A.D. Martin, *Phys. Rev.* **D57** (1998) 496.

[19] J. Bartels, V. Del Duca, A. De Roeck, D. Graudenz and M. Wüsthoff, *Phys. Lett.* **B384** (1996) 300.

[20] E. Mirkes and D. Zeppenfeld, *Phys. Rev. Lett.* **78** 428 (1997).

[21] G. Kramer and B. Pötter, hep-ph/9901314.

[22] H. Jung, L. Jönsson and H. Küster, hep-ph/9811368; hep-ph/9903306.

[23] G.A. Schuler and T. Sjöstrand, *Phys. Lett.* **B376** (1996) 193.